42nd AIAA/ASME/SAE/ASEE Joint Propulsion Conference & Exhibit AIAA-2006-4658
9-12 July, 2006, Sacramento, CA

Heavy Particle Velocity and Electron Mobility Modeling in Hybrid-PIC Hall Thruster Simulations

Richard R. Hofer,* Ira Katz,† Ioannis G. Mikellides,‡ and Manuel Gamero-Castaño§
Jet Propulsion Laboratory, California Institute of Technology, Pasadena, CA 91109

The primary life-limiting mechanism in Hall thrusters is the erosion of the discharge chamber walls by propellant ions. Although substantial progress has been made in recent years in Hall thruster theory and design, relatively little progress has been made in understanding this life limiting process. The development of this understanding is critically needed if Hall thrusters are to be successfully integrated into NASA science missions. In this paper, we review recent progress of the development of physics-based modeling tools aimed at predicting the service life of Hall thrusters. A channel erosion sub-model developed at the Jet Propulsion Laboratory (JPL) is combined with results from the 2-D hybrid fluid/particle-in-cell computer code HPHall-2 that is used to simulate the plasma and neutral gas inside the discharge chamber and near-plume regions. This paper assesses the impact of the heavy particle velocity and electron mobility models on plasma simulations. It is found that improvements on the velocity condition at the injector boundary and on the gas-surface interaction model for neutrals and ions at wall boundaries leads to neutral speeds and mass utilization efficiencies that are more consistent with experimental values. Simulations using non-classical electron mobility that is wall-dominated inside the channel but Bohm-dominated in the near plume yield more accurate electron temperature and electric field distributions along the channel but at lower values typically obtained in experiments.

---

* Member of the Technical Staff, Advanced Propulsion Technology Group, Propulsion and Materials Engineering Section, 4800 Oak Grove Drive, Mail Stop 125-109; richard.r.hofer@jpl.nasa.gov. Member AIAA.

† Group Supervisor, Advanced Propulsion Technology Group, Propulsion and Materials Engineering Section. Senior Member AIAA.

‡ Member of the Technical Staff, Advanced Propulsion Technology Group, Propulsion and Materials Engineering Section. Senior Member AIAA.

§ Member of the Technical Staff, Advanced Propulsion Technology Group, Propulsion and Materials Engineering Section. Senior Member AIAA.

I. Introduction

SINCE its inception over four decades ago, the Hall thruster's unique combination of high specific impulse and thrust-to-power ratio established it as a favored propulsion system for a variety of near-Earth space missions. Over 238 Hall thrusters from the Russian Experimental Design Bureau Fakel, 128 of which have been SPT-100s, have flown in space since the early 1970s on Russian, European, and American spacecraft [1,2]. The European Space Agency recently demonstrated Hall thrusters for primary propulsion on the lunar orbiting SMART-1 spacecraft [3]. This spacecraft used a Snecma 1.5 kW PPS-1350-G and has set several new endurance records for the in-space use of Hall thruster technology.

The 1998 launch of a TsNIIMASH D-55 on the National Reconnaissance Office's Space Technology Experiment Satellite (STEX) marked the first Hall thruster flight on a United States (US) spacecraft [4]. Today, commercial Hall thrusters are available in the US from Aerojet, Busek, and International Space Technologies Incorporated (ISTI). The first commercial use of Hall thrusters by a US spacecraft manufacturer was on Space Systems/Loral's (SS/L) MBSAT (2004) [1]. SS/L has subsequently flown Hall thrusters on Intelstar Americas-8 (2005), and iPSTAR-1 (2005). Busek will likely be the first to demonstrate American Hall thruster technology when the 200 W BHT-200 flies on board the TacSat-2 spacecraft in late 2006 [5,6]. Domestically-developed Aerojet BPT-4000 Hall thrusters are scheduled to begin flying on Lockheed Martin Space Systems Company GEO satellites in 2008 [7,8]. Commercial options such as these offer an opportunity for significant cost reductions on many science missions now being considered by NASA. Through procurements from existing product lines the cost associated with the infrequent development of thruster components for science missions may be significantly reduced [9,10].

Many NASA science missions, such as those considered under the cost-capped Discovery program for example, require wider throttling capabilities and longer thruster life compared to commercial applications [9,10]. The service life of electric propulsion has been customarily demonstrated through life ground tests that typically cost several million dollars. The Extended Life Test of the 2.3 kW NSTAR ion thruster was completed in 2004 after more than 30,000 h of operation at the Jet Propulsion Laboratory (JPL), and was the longest life test of an ion thruster ever conducted [11]. In 2005, Aerojet demonstrated more than 5,800 h of operation of a BPT-4000 as part of a qualification program for geosynchronous earth orbit (GEO) applications [7,8]. The potential benefits for Discovery-class missions prompted NASA to fund a low-power life test extension of this thruster [12]. As NASA missions become more demanding both the cost and time associated with life tests is expected to rise. While some NASA missions may be able to absorb such costs, launch window opportunities and mission timelines may simply rule out long-duration life testing.

A rigorous life-modeling program has been ongoing at JPL since 2003 in an effort to establish a thruster life qualification capability that will decrease the cost and time required to assess thruster service life. The reasoning and motivation behind the life-modeling effort are based on the premise that the physics that drive thruster degradation need only be identified and modeled once. Once the appropriate physics models have been developed and validated then it becomes a matter of model parameterization to

quantify the wear expected in any given thruster. Moreover, for most conventional ion and Hall thrusters, life models may be validated by relatively simple and inexpensive experiments and/or by existing data, and can then be applied to more complex systems, before they are built, to predict life thus saving cost and time.

Two major life-limiting mechanisms exist in Hall thrusters: erosion of the discharge chamber walls and erosion of the neutralizer hollow cathode. To better understand these mechanisms the computational effort at JPL has made use of existing models [13,14] wherever applicable, and has developed new models as deemed necessary [15,16]. In this paper, we report on our recent efforts to model discharge chamber erosion. This is a continuation of previous work reported recently by Gamero-Castaño and Katz [17] that utilized a modified version of the 2D computer code, HPHall-1, originally developed by Fife and Martínez-Sánchez [13]. HPHall employs a hybrid fluid/particle-in-cell (PIC) numerical approach to simulate the evolution of the plasma and neutral gas inside the discharge chamber and near plume regions of a Hall thruster. Parra and Ahedo have recently provided several improvements to the code [14], resulting in the latest release, HPHALL-2. Throughout this paper, we report results using HPHALL-2 with additional JPL modifications.

Erosion of the discharge chamber is caused by energetic propellant ions. Hence, the accurate determination of the channel recession as a function of time requires knowledge of the plasma properties inside the channel as well as the sputtering yield of the dielectric material. Gamero-Castaño and Katz employed a sputtering yield based on Tamamura's model for the sputtering of monatomic elements [18], together with experimental data reported by Garnier [19] to self-consistently compute the channel recession during operation of an SPT-100 [17]. Here, we report on improvements made to the heavy particle velocity and electron mobility models in HPHall-2. Specifically, we discuss improvements on the velocity condition at the injector boundary and on the gas-surface interaction model of neutrals and ions at wall boundaries. The electron mobility model in HPHALL-2 has also been upgraded similar to results obtained by Hagelaar, et al. and Koo, et al. [20,21], which suggest that anomalous mobility in Hall thrusters is driven by wall collisionality inside the channel and by magnetic field effects (Bohm neoclassical) in the near-plume region. The impact of these changes on the plasma properties is assessed.

II. Model Inputs

All results in this paper are based on the SPT-100 geometry and magnetic field used previously in Ref. [17]. Figure 1 shows the geometry and grid and Table 1 presents some of the basic inputs used for the simulations. We have updated the anode and wall temperatures from those used in Ref. [17] to values found in the literature [22,23]. Modifications specific to code updates, such as the wall accommodation, are discussed later.

Results are typically obtained by first populating the discharge chamber with neutrals for 20K iterations (N=0-20K) in HPHALLs "neutral only" mode. For simulations concerned with examining the neutral dynamics only, an additional 20K iterations (N=20-40K) are then run, from which average results are computed. For plasma simulations, the initial 20K neutral runs are used as inputs for 10K iterations

(N=20-30K) with the plasma on in order to get past the initial startup transients. Finally, 20K iterations (N=30-50K) are run again with the plasma, from which average results are computed. Small changes to model inputs can also be examined by using previously converged results by running for 20K iterations (N=50-70K), then running an additional 20K iterations (N=70-90K) to be sure that the time history of the input changes are no longer affecting the solution.

Table 1. HPHALL inputs for SPT-100 simulations.

Parameter	Value
Discharge Voltage (V)	300
Mass flow rate (mg/s)	5
Anode temperature (K), [22,23]	750
Wall temperature (K), [22,23]	850
Channel outer diameter (mm)	100
Channel width (mm)	15
Channel length (mm)	25
Simulation time step (s)	5e-8

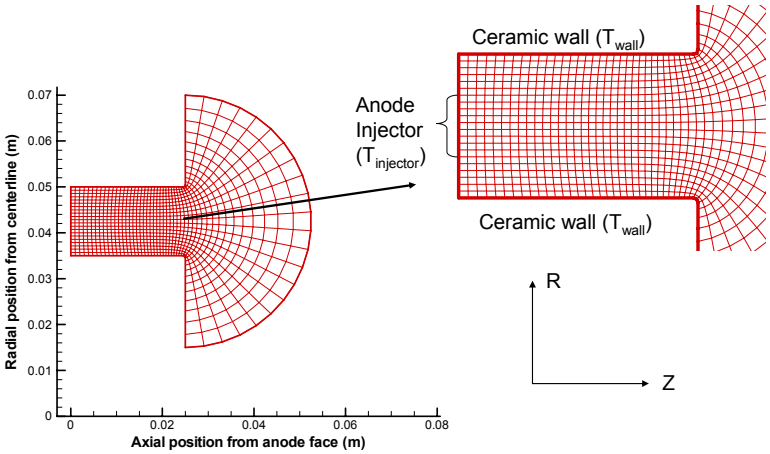

Figure 1. Geometry and grid used for SPT-100 simulations with HPHALL.

III. Heavy Particle Velocity Modeling

Heavy particle velocities are sampled at model boundaries representing the anode injector and discharge chamber walls. The code accounts for particle injection, reflection, and recombination. At the anode, neutrals are randomly placed at the injector location after sampling a prescribed distribution function defined by the anode temperature and a drift velocity normal to the injector surface. Ions are sampled identically to neutrals if pre-ionization is used, but this option is not used in any of our simulations. At the walls, neutrals impacting the walls are re-emitted after applying a wall accommodation factor. Ions are handled the same way as neutrals with some additional steps to account

for the mass disparity of the neutral and ion macroparticles [14]. When re-emitted, ions impacting the walls are recombined into neutrals.

We have modified HPHALL-2 with the following changes:

1. In order to more accurately model realistic anode injectors, the anode injection has been modified to allow for a user selectable injection velocity normal to the anode surface.
2. The gas-surface interaction model has been updated from previous HPHALL versions.

Each of these modifications are discussed below.

A. Gas-Surface Interactions

Since the original version of HPHALL [13], the temperature of heavy particles reflected from wall boundaries has been given by a weighted average of the wall and impact temperatures given by

$$T_{emi} = a_w T_w + (1 - a_w) T_{imp} \,, \tag{1}$$

where a_w is a wall accommodation coefficient, T_w is the wall temperature, T_{imp} is the incoming particle temperature, and T_{emi} is the emitted particle temperature. HPHALL applies separate accommodation coefficient for ions and neutrals, with default values of 0.8 for both.

The motivation for the gas-surface interaction model given by Eqn. (1) is unclear and does not reflect models commonly found in the literature. The model usually adopted in simulations, sometimes called the Maxwell scattering model [24], assumes that some fraction of particles a_w impacting a solid surface are reflected diffusely at the wall temperature, with the remainder (1- a_w) being reflected specularly (i.e., their tangential velocities are reversed while the normal component is unchanged) with no change in temperature. The Maxwell scattering model assumes then that the reflected particles retain only the (1- a_w) fraction of their incoming state.

We have updated the code to use the Maxwell scattering model by implementing the following algorithm in our version of the code, which will be referred to as HPHALL-2-JPL throughout this paper:

1. For each incoming particle, a random fraction R_f is generated.
2. If R_f is less than a_w, the particle is reflected diffusely.
3. If R_f is greater than or equal to a_w, the particle is reflected specularly.

Experiments indicate that complete diffuse reflection (a_w=1), or perfect accommodation, adequately describes the gas-surface interaction for "engineering" surfaces [25]. This occurs primarily due to surface roughness effects that tend to randomize the distribution of reflected particles, which is the likely case for the ceramic discharge chambers in Hall thrusters that are subject to sputtering and redeposition. In our simulations, we have opted to set the wall accommodation coefficient to unity for both neutrals and ions.

B. Velocity Sampling of Reflected Heavy Particles

At the walls, velocities are sampled at surfaces from half-Maxwellian distribution functions, while at the anode a drifting half-Maxwellian is sampled with a user selectable drift velocity. Direct sampling methods are used when the drift velocity is zero, while an acceptance-rejection technique is applied for

non-zero drifts [25]. The acceptance-rejection technique is required because the cumulative distribution function (CDF) of a drifting half-Maxwellian is not invertible.

For the injector and the walls, we will choose to work in cylindrical coordinates with the axial component z aligned with the unit normal of the surface and the radial r and azimuthal θ components in the plane tangent to the surface. These coordinate definitions are shown in Figure 2.

$$v_x = v_r \cos\theta \qquad v_r^2 = v_x^2 + v_y^2$$
$$v_y = v_r \sin\theta \qquad d^3r = rd\theta dr dz$$
$$v_z = v_z$$

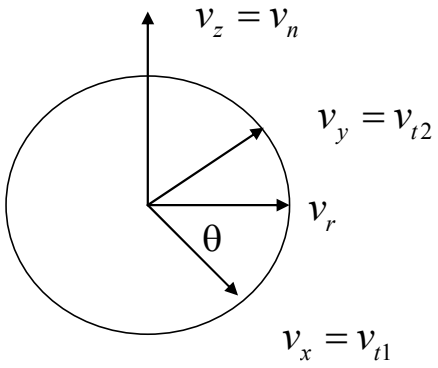

Figure 2. Coordinate system used for velocity sampling.

We seek to find the average velocity of the inward flux of neutrals across a surface element given by [25,26]

$$\langle \vec{v} \rangle = \frac{\beta^3}{\pi^{3/2}} \int_{-\infty}^{\infty} dv_x \int_{-\infty}^{\infty} dv_y \int_{0}^{\infty} dv_z \left(v_z \exp\left(-\beta^2 \left(v_x^2 + v_y^2 + v_z^2 \right) \right) \right) \qquad \text{Cartesian}$$
$$= \frac{\beta^3}{\pi^{3/2}} \int_{0}^{2\pi} d\theta \int_{0}^{\infty} dv_r \left(v_r \exp\left(-\beta^2 v_r^2 \right) \right) \int_{0}^{\infty} dv_z \left(v_z \exp\left(-\beta^2 v_z^2 \right) \right) \qquad \text{Cylindrical} \quad , \tag{2}$$

where β is related to the most-probable speed by

$$\frac{1}{\beta} = v_{mp} = \sqrt{\frac{2kT_e}{m}} \quad . \tag{3}$$

For each component f of the distribution, we require

$$\int_a^b f(x)dx = 1 \,, \tag{4}$$

and we need to find the CDF F given by

$$F(x) = \int_a^x f(x)dx \qquad F \in [0,1] \,, \tag{5}$$

such that the distribution function can be sampled by inversion according to

$$F(x) = R_f = \text{ Random Fraction} \qquad R_f \in [0,1] \,. \tag{6}$$

At all surfaces, the tangential velocity components are directly sampled from the 2D thermal Maxwellian distributions defined by r and θ. In the tangential plane, θ is uniformly distributed such that

$$\theta = 2\pi R_{f1} \qquad R_{f1} = \text{ First Random Number } \in [0,1]. \tag{7}$$

The CDF for the radial component is given by

$$F_{\beta^2 r^2} = 1 - \exp\left(-\beta^2 r^2\right) \Rightarrow r = \sqrt{-\ln\left(R_{f2}\right)}\Big/\beta \qquad R_{f2} = \text{ Second Random Number } \in [0,1], \tag{8}$$

such that the tangential velocity components are given by

$$\begin{aligned} v_x &= v_{mp}\sqrt{-\ln\left(R_{f2}\right)}\cos\left(2\pi R_{f1}\right) \\ v_y &= v_{mp}\sqrt{-\ln\left(R_{f2}\right)}\sin\left(2\pi R_{f1}\right) \end{aligned}. \tag{9}$$

Since the functional form of the normal component is identical to the r component we have

$$v_n = v_{mp}\sqrt{-\ln\left(R_{f3}\right)} \quad R_{f3} = \text{ Third Random Number } \in [0,1]. \tag{10}$$

If instead, the normal component has a directed drift velocity given by

$$\underbrace{v_n}_{\substack{\text{total} \\ \text{velocity}}} = \underbrace{v_n'}_{\substack{\text{thermal} \\ \text{velocity}}} + \underbrace{u_d}_{\substack{\text{drift} \\ \text{velocity}}}, \tag{11}$$

then the CDF is no longer invertible. To show this, it is convenient to define

$$\begin{aligned} s &= \beta u_d = \text{ Drift Speed Ratio} \\ M &= \beta v_n = \text{ Most Probable Speed Ratio} \end{aligned}. \tag{12}$$

The tangential sampling is unaffected, while the normal component becomes

$$\langle v_n \rangle = \frac{\beta}{\sqrt{\pi}} \int_0^\infty v_z \exp\left(-\beta^2 \left(v_n - u_d\right)^2\right) dv_z = \frac{1}{\sqrt{\pi}} \int_0^\infty M \exp\left(-\left(M - s\right)^2\right) dM \,. \tag{13}$$

The function given by

$$f \sim M \exp\left(-\left(M - s\right)^2\right), \tag{14}$$

has a CDF given by

$$F\left(M\right) = \frac{e^{-s^2} + s\sqrt{\pi}\left(Erf\left(M - s\right) + Erf\left(s\right)\right) - e^{-(M-s)^2}}{e^{-s^2} + s\sqrt{\pi}\left(1 + Erf\left(s\right)\right)}. \tag{15}$$

This function is not invertible, so direct sampling is not possible. Instead, the acceptance-rejection technique is used [25]. To use acceptance-rejection, the distribution function f is normalized by its maximum f_{max} and then the ratio $f'=f/f_{max}$ is formed. The result is

$$f' = \frac{f}{f_{\max}} = \frac{2M}{s + \sqrt{2 + s^2}} \exp\left(-\left(M - s\right)^2 + \frac{1}{2} + \frac{s}{2}\left(s - \sqrt{2 + s^2}\right)\right). \tag{16}$$

In HPHALL-2-JPL, the acceptance-rejection technique is only used if a non-zero drift velocity is imposed at the anode injector.

C. Results

Using the derivations above, the neutral and ion sampling routines at boundaries in HPHALL-2-JPL are implemented in the following ways:

1. Variable neutral and ion wall accommodation coefficients. (Default: $a_w = 1$, diffuse reflection)
2. Variable normal drift speed at the anode injector. (Default: *M=0*). The case *M=1* is identical to the current HPHALL-2 implementation.
3. Direct sampling at the walls. This is unchanged from HPHALL-2.

The implementation of a user selectable anode injection speed allows for less than ideal anode designs. Anodes are typically constructed to mimic a thermal half-Maxwellian as much as possible so that the neutral residence time in the discharge chamber is maximized (and hence, the ionization rate). Fluid expansion effects and space limitations may prohibit this from occurring completely. Interestingly, there are very few sources in the literature that have considered these effects, despite the impact on thruster stability, thermal margin, performance and lifetime.

Comparisons were performed between HPHALL-JPL [17], HPHALL-2 [14], and HPHALL-2-JPL. Neutral density and speed contours are compared in Figure 3 and Figure 4, respectively, for neutral only simulations (plasma off). As expected, the updates in HPHALL-2 result in slower neutrals speeds and more uniform density across the channel.

Table 2 compares neutral density, neutral speed, and mass utilization efficiency for the various HPHALL versions from neutral only and plasma simulations. Values for speed and density in the table were generated by sampling at the exit plane on channel centerline. When the anode injection is sonic, we see that the HPHALL-2 updates reduce the neutral speed from 280 to 264 m/s for the neutral only simulations and from 593 to 325 m/s for the plasma simulations. The substantial difference in the neutral speed during plasma simulations results in a 9.1% (absolute) increase in mass utilization from 79.7% to 88.8%. Since neutral speeds of 300 m/s and mass utilization efficiencies of 90% are consistent with experimental measurements [27-29], we conclude that the HPHALL-2 updates are more representative of Hall thruster operation.

Figure 5, Figure 6, and Figure 7 compare results from HPHALL-2-JPL for zero (M=0) and sonic (M=1) neutral injection speeds. (Figure 6 and Figure 7 are the same data plotted over different range of values.) Sonic injection leads to lower density and faster speeds, as expected. Table 2 also shows the effects of anode injection speed. Changing the anode injection from sonic to zero results in a 24-26 m/s decrease in neutral speed and a 1.3% increase in mass utilization to 90.1%.

From all of these results, we conclude that updating the gas-surface interaction model is largely responsible for the significant change in mass utilization between the versions of the code. We expect these updates to significantly improve the accuracy of erosion simulations. Erosion simulations with the heavy particle model updates will be conducted next.

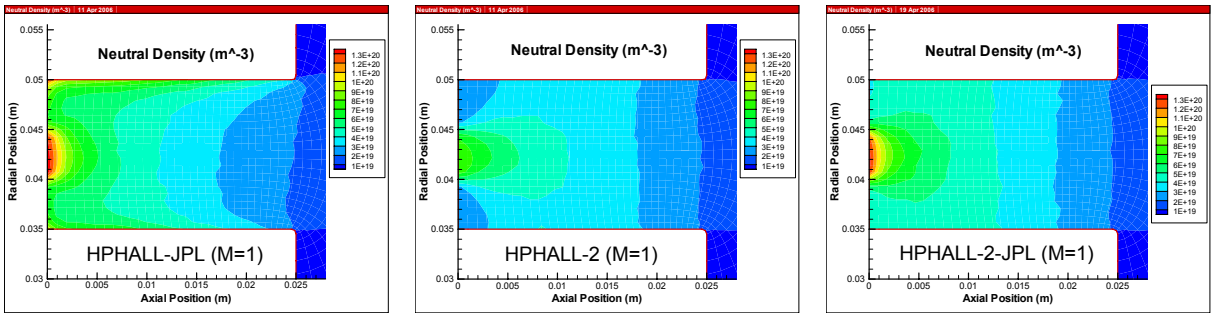

Figure 3. Neutral density in the SPT-100 discharge chamber for the various versions of HPHALL in neutral only mode (plasma off). (n_n ∈ [1e19, 1.3e20] 1/m^3)

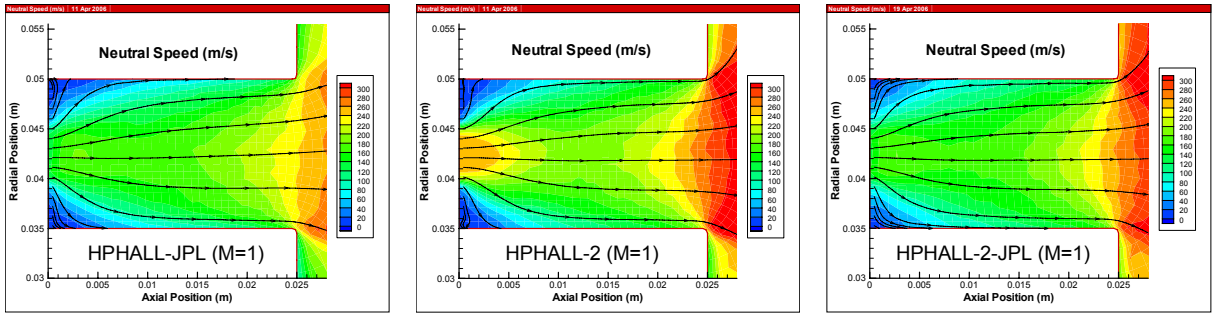

Figure 4. Neutral speed and velocity streamlines in the SPT-100 discharge chamber for the various versions of HPHALL in neutral only mode (plasma off). (v_n ∈ [0, 300] m/s)

Table 2. Neutral speed, neutral density, and mass utilization efficiency for the various HPHALL versions from neutral only and plasma simulations.

	Neutral Only Mode		Plasma Mode		
	v_n (m/s)	n_n (1/m^3)	v_n (m/s)	n_n (1/m^3)	Mass utilization efficiency
HPHALL-1-JPL M=1	239	2.0 x 10^{19}	758	1.1 x 10^{18}	75.9%
HPHALL-2 M=1	280	1.9 x 10^{19}	593	1.6 x 10^{18}	79.7%
HPHALL-2-JPL M=1	264	1.9 x 10^{19}	325	1.4 x 10^{18}	88.8%
HPHALL-2-JPL M=0	240	2.0 x 10^{19}	299	1.2 x 10^{18}	90.1%
* Speed and density values sampled at exit plane on channel centerline					

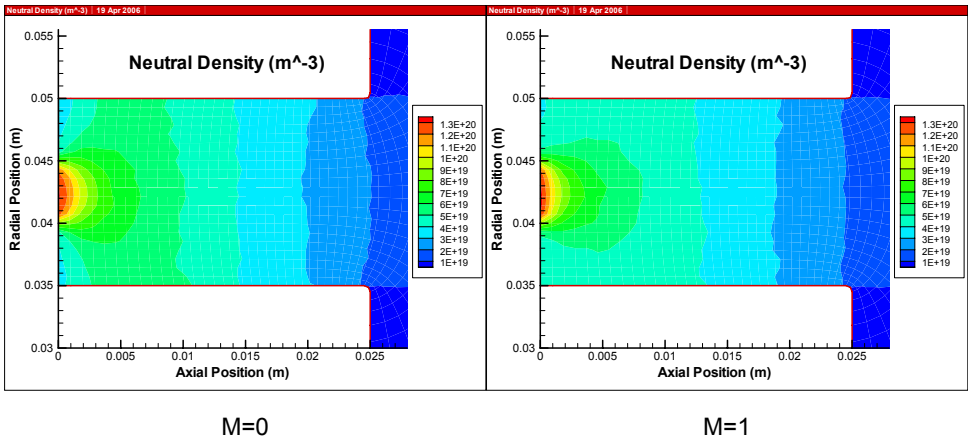

Figure 5. Neutral density from HPHALL-2-JPL for the case of zero (M=0) and sonic (M=1) axial drift velocities in neutral only mode (plasma off). ($n_n \in$ [1e19, 1.3e20] 1/m^3)

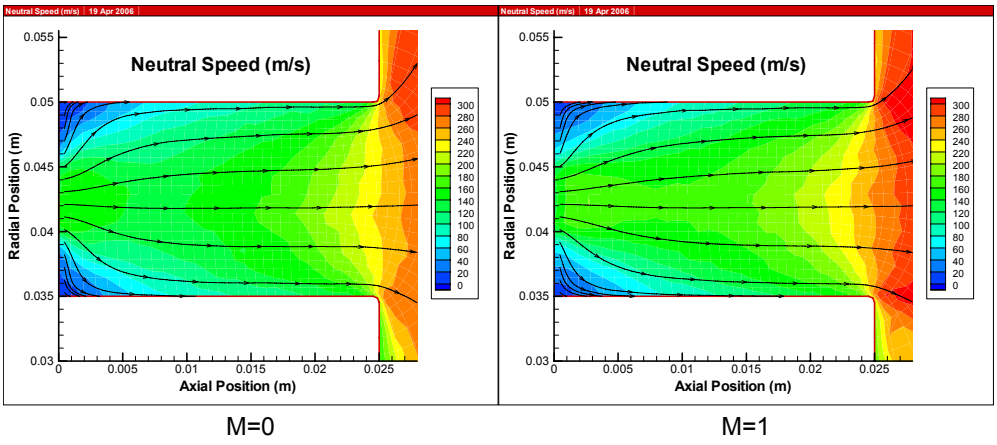

Figure 6. Neutral speed and velocity streamlines from HPHALL-2-JPL for the case of zero and sonic axial drift velocities in neutral only mode (plasma off). ($v_n \in$ [0, 300] m/s)

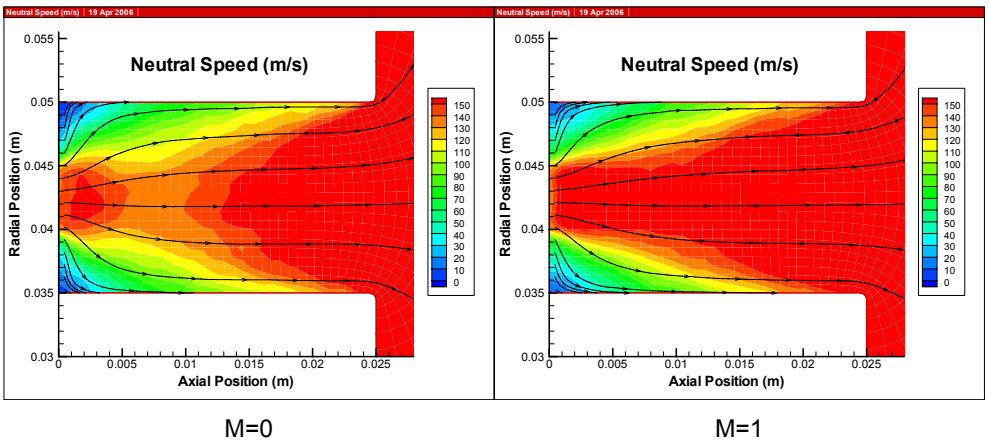

Figure 7. Neutral speed and velocity streamlines from HPHALL-2-JPL for the case of zero and sonic axial drift velocities in neutral only mode (plasma off). ($v_n \in$ [0, 150] m/s)

IV. Electron Mobility Modeling

A. Background

The classical formulation of the axial, or cross-field, electron mobility is given by

$$\mu_{ez} = \frac{e}{\nu_e m_e}\left(\frac{1}{1+\Omega_e^2}\right), \tag{17}$$

which can be simplified to

$$\mu_{ez} \approx \frac{e}{\nu_e m_e \Omega_e^2} = \frac{\nu_e m_e}{eB_r^2} \quad , \tag{18}$$

since the electron Hall parameter is much greater than unity throughout the discharge chamber [30,31].

Measurements of the electron current in Hall thrusters have shown that the effective electron collision frequency in an SPT-100 is on the order of 10^7-10^8 s^{-1} [30-32]. A collision frequency based off "classical" collisions between the electrons and the heavy particles cannot account for this high a value of collision frequency. Estimates inferred from global measurements of the electron current [30-32], as well as calculations based directly from internal plasma measurements [33,34], show that the classical collision frequency is on the order of 10^6-10^7 s^{-1}. Thus, additional "anomalous" transport mechanisms must be present that enhance the cross-field electron mobility.

Two mechanisms that could be responsible for anomalous transport are collisions with the walls and turbulent plasma fluctuations. Determining which of these mechanisms is dominant has been the subject of considerable debate since the 1960s. However, experimental, numerical simulation, and theoretical research [13,20,21,30-46], shows that it is likely that both mechanisms each play a role in different regions of the discharge chamber and at different thruster operating conditions. Including these effects in the mobility can be accomplished by using an effective electron collision frequency that is sometimes modeled as

$$\nu_e = \nu_{eff} = \nu_{en} + \nu_{wall} + \nu_{turb}\,, \tag{19}$$

where ν_{en} is the electron-neutral collision frequency, ν_{wall} is the collision frequency of the electrons with the walls, and ν_{turb} is a collision frequency due to turbulent plasma fluctuations (i.e., anomalous Bohm diffusion). The electron-electron collision frequency ν_{ee} and the electron-ion collision frequency ν_{ei} are absent from Eqn. (19). This is because these collision frequencies, which are typically an order of magnitude less than the electron-neutral collision frequency [34], are usually neglected for the sake of computational expediency [30].

Morosov, et al. [37] first suggested that wall collisions have a role in enhancing cross-field transport by introducing the concept of "near-wall conductivity." In this view, the walls act as a macroparticle on which primary electrons may also collide. Reflection of primary electrons and the emission of low-energy secondary electrons from the walls act to enhance the bulk electron conductivity by untrapping electrons from magnetic field lines and increasing the axial electron current. Near-wall conductivity has been

extensively studied in experiments, numerical simulations, and theoretically [30-32,38-40,42]. This research has shown that near-wall conductivity plays a role in enhancing the effective collision frequency.

The experiments of Janes and Lowder [44] were the first to demonstrate that azimuthal fluctuations in the electric field correlated with density gradients could account for anomalous diffusion via adiabatic ExB drifts. Anomalous diffusion of this sort was found to agree closely with Bohm-like mobility, which scales as the inverse of the magnetic field. Meezan, et al. [45,46] have also studied the effects of field fluctuations in a low-voltage (100-200 V) Hall discharge with alumina walls and a long channel and also found that Bohm-like mobility could explain the observed cross-field transport. However, as pointed out by Ahedo et al. [32], Bohm-like diffusion likely dominates at low-voltage because the electron temperature is much lower, thereby reducing the wall collision rate. Anomalous Bohm-like diffusion can be included in the expression for the effective collision frequency (Eqn. (19)) by supposing

$$\nu_{turb} = \alpha_{ano}\omega_{ce}\,, \tag{20}$$

where α_{ano} is a parameter that can be adjusted so that the necessary amount of cross-field diffusion results. In the case of classic Bohm diffusion, α_{ano} would be equal to 1/16 (i.e., if Bohm transport dominates the Hall parameter would be $\Omega_e = \alpha_{ano}^{-1} = 16$).

In practice, assuming only near-wall conductivity or Bohm-like diffusion throughout the channel is poorly justified by the available data. This was shown from experiments by Haas [34] and computations by Choueiri [33] using Bishaev and Kim's data [41]. Haas' experiments were conducted on the UM/AFRL P5 Hall thruster. Haas showed that the effective Hall parameter in the ExB drift region near the exit plane can approach that given by classical collisions alone, but falls to the Bohm value near the anode and downstream of the exit plane. This strongly suggests that a mixed mobility model, accounting for both Bohm-like and wall collisionality effects, is more appropriate.

Fife was among the first to adopt such an approach in numerical simulations, by accounting for classical scattering and Bohm-like diffusion in a simulation of the SPT-70 using the original HPHALL [13]. Fife found that a value of $\alpha_{ano}^{-1} = 107$ yielded a sufficient amount of cross-field transport. Ahedo, et al. [32] has also found acceptable results when $\alpha_{ano}^{-1} = 100$ in a mixed mobility approach that accounted for classical scattering, wall collisions, and Bohm-like diffusion. Updates in HPHALL-2 by Parra and Ahedo also account for classical scattering, wall collisions, and Bohm-like diffusion [14]. The value of α_{ano}^{-1} used by Fife and Ahedo, et al. agree (within an order of magnitude) with those found experimentally, which have shown that the electron Hall parameter attains a value of several hundred in the closed-drift region [34,41,47]. Recent measurements by Hofer [27] have also shown that the electron Hall parameter in a high-efficiency, high-specific impulse Hall thruster averaged 160 over a voltage range of 400-900 V. Others have adopted similar mixed mobility approaches that have differed by which of the terms shown in Eqn. (19) are included in simulations [20,21,30,40,42].

B. Results

We are investigating methods to improve the electron mobility model that is currently implemented in HPHALL-2. Similar to the heavy particle velocity updates, mobility models that more closely mimic experimental results found in the literature should lead to more accurate erosion predictions.

The mobility model presently in HPHALL-2 applies the terms due to classical and Bohm mobility in Eq. (19) throughout the simulation domain while the wall term is used only in the discharge chamber. Hagelaar, et al. and Koo, et al. [20,21] have implemented a similar approach, except the Bohm mobility term is applied only in the plume region downstream of the discharge chamber exit. This is approach can be justified by results from Morosov, et al. [48] that have shown how flowing plasma in the presence of decreasing magnetic field gradients can be unstable and by experimental measurements of the axial distribution of the electron Hall parameter [34]. We have performed simulations to evaluate how the approach taken by Hagelaar and Koo affect results from HPHALL-2-JPL (i.e., with the heavy particle modeling updates described above).

Figure 8 and Figure 9 compares electron temperature and axial electric field predictions from HPHALL-2-JPL with the standard mobility model of HPHALL-2 and the mixed mobility model described above. The standard model predicts peak electron temperature and electric field strengths downstream of the exit plane, which is not consistent with experimental data [34]. The mixed mobility model more correctly places the peak electron temperature and electric field inside the discharge chamber, but results in a decrease in the peak electron temperature from 30 eV with the standard model to 18 eV with the mixed model. While the spatial trends are more consistent with experiment, the electron temperature is lower than expected (experiments typically report peak electron temperatures that are around 10% of the discharge voltage) [34].

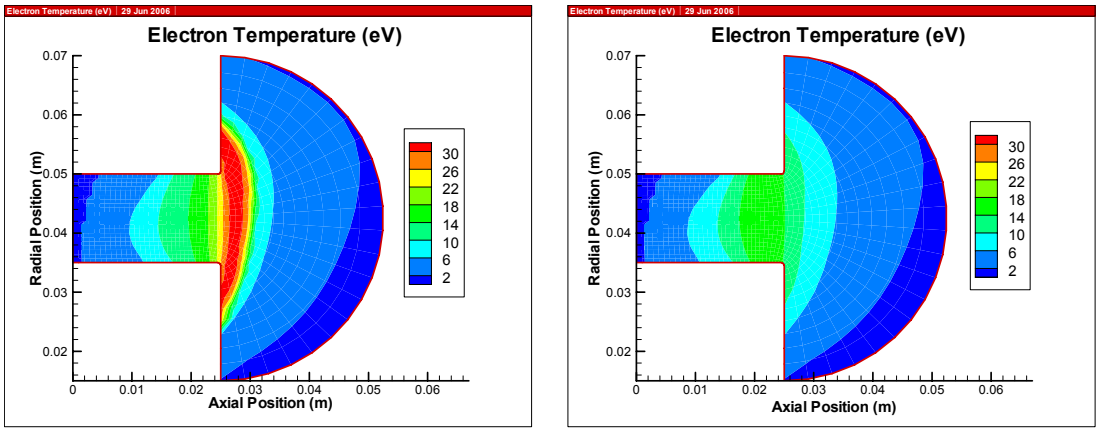

Standard Mobility Model | Mixed Mobility Model

Figure 8. Electron temperature contours from HPHALL-2-JPL with different mobility models. ($T_e \in [2, 30]$ eV)

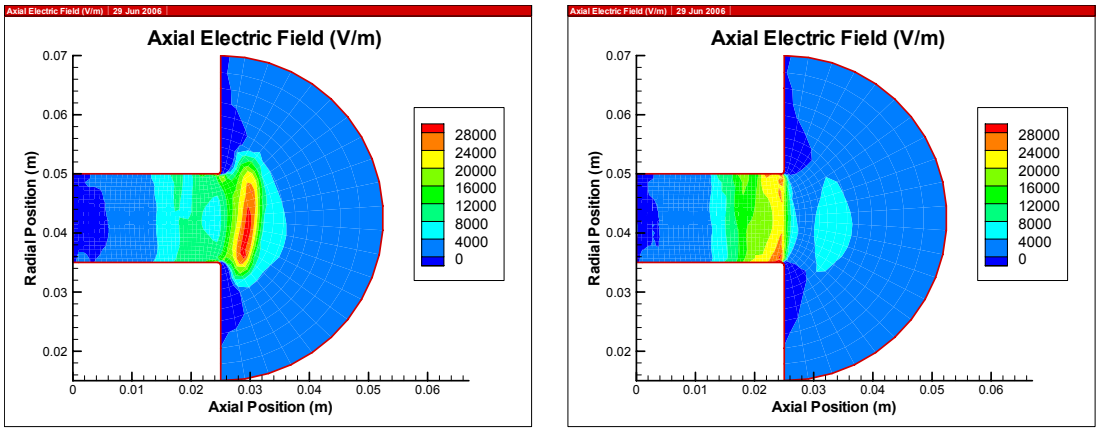

Standard Mobility Model | Mixed Mobility Model

Figure 9. Electric field contours from HPHALL-2-JPL with different mobility models. ($E_z \in [0, 28000]$ V/m)

Erosion calculations from Ref. [17] using HPHALL-1-JPL predicted a shorter axial length for the erosion zone than results from experiment. This is shown in Figure 10, which shows results from Ref. [17] of erosion in the SPT-100. We expect the improvements in spatial positioning of both the electron temperature and electric field distributions shown in Figure 8 and Figure 9 to improve the erosion calculations by more accurately placing the start of the erosion zone in the discharge chamber. We are presently continuing our studies of mixed mobility models, with the goal of more precisely predicting the distribution of electron temperature and other plasma properties throughout the discharge chamber.

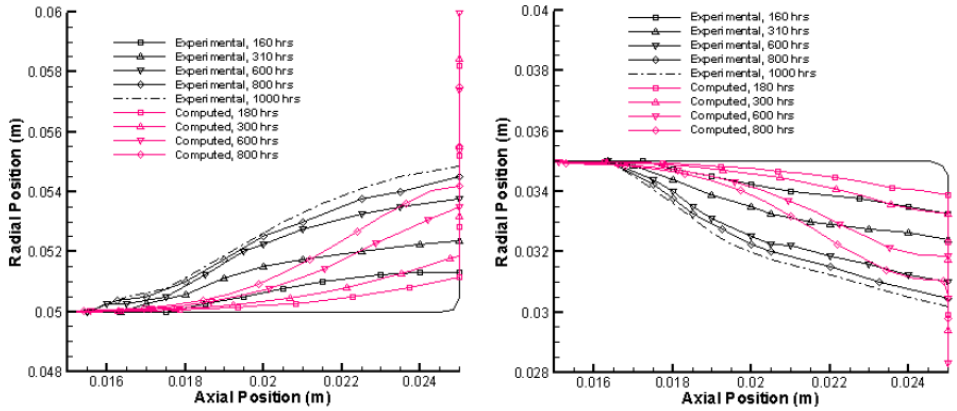

Figure 10. Computed and experimental erosion profiles for the outer and inner discharge chamber walls from Ref. [17].

V. Conclusion

Updates to HPHALL-2 of the heavy particle velocity model have resulted in decreased neutral speeds and increased mass utilization that are more consistent with values found experimentally. Numerical experiments with the electron mobility model have also shown how implementing a model closer to that

observed in experiments yields more realistic electron temperature and electric field distributions along the channel but at lower values typically obtained in experiments. We are presently investigating how these changes impact the accuracy of erosion predictions. In the near future, HPHALL-2 and JPLs erosion submodel will be applied to an updated magnetic field profile of the SPT-100, the Aerojet BPT-4000, and the NASA HIVHAC thruster.

Acknowledgments

The research described in this paper was carried out at the Jet Propulsion Laboratory, California Institute of Technology, under a contract with the National Aeronautics and Space Administration. Support of this work was provided by the NASA In-Space Propulsion program and was managed by Randy Baggett (MSFC), technology area manager for Solar Electric Propulsion.

References

[1] Pidgeon, D. J., Corey, R. L., Sauer, B., and Day, M. L., "Two Years on-Orbit Performance of SPT-100 Electric Propulsion," Presented at the 24th AIAA International Communications Satellite Systems Conference, AIAA Paper 2006-5353, San Diego, CA, June 11-14, 2006.

[2] Kim, V., Popov, G., Arkhipov, B., Murashko, V., Gorshkov, O. et al., "Electric Propulsion Activity in Russia," Presented at the 27th International Electric Propulsion Conference, IEPC Paper 2001-005, Pasadena, CA, Oct. 15-19, 2001.

[3] Koppel, C. R. and Estublier, D., "The SMART-1 Hall Effect Thruster around the Moon: In Flight Experience," Presented at the 29th International Electric Propulsion Conference, IEPC Paper 2005-119, Princeton, NJ, Oct. 31-Nov. 4, 2005.

[4] Naval Research Laboratory, "National Reconnaissance Office Satellite Successfully Launched," Press Release, http://www.nro.gov/PressReleases/prs_rel25.html, Oct. 3, 1998.

[5] Yee, T., "Roadrunner, a High-Performance Responsive Space Mission," Presented at the 18th AIAA/USU conference on small satellites, SSC04-I-5, Logan, UT, Aug., 2004.

[6] Bromaghim, D. R., Singleton, J. T., Gorecki, R., Dong Tan, F., Choy, H. et al., "200 W Hall Thruster Propulsion Subsystem Development for Microsatellite Missions," Presented at the 53rd JANNAF Propulsion Meeting, Monterey, CA, Dec. 5-8, 2005.

[7] de Grys, K. H., Welander, B., Dimicco, J., Wenzel, S., Kay, B. et al., "4.5 kW Hall Thruster System Qualification Status," Presented at the 41st AIAA/ASME/SAE/ASEE Joint Propulsion Conference, AIAA Paper 2005-3682, Tucson, AZ, July 10-13, 2005.

[8] Welander, B. A. and de Grys, K. H., "Completion of the BPT-4000 Hall Thruster Qualification," Presented at the 53rd JANNAF Propulsion Meeting, Monterey, CA, Dec. 5-8, 2005.

[9] Hofer, R. R., Randolph, T. M., Oh, D. Y., Snyder, J. S., and de Grys, K. H., "Evaluation of a 4.5 kW Commercial Hall Thruster System for NASA Science Missions," Presented at the 42nd AIAA/ASME/SAE/ASEE Joint Propulsion Conference, AIAA Paper 2006-4469, Sacramento, CA, July 9-12, 2006.

[10] Oh, D. Y. and Goebel, D. M., "Performance Evaluation of an Expanded Throttle Range XIPS Ion Thruster System for NASA Science Missions," Presented at the 42nd AIAA/ASME/SAE/ASEE Joint Propulsion Conference, AIAA Paper 2006-4466, Sacramento, CA, July 9-12, 2006.

[11] Sengupta, A., Brophy, J. R., Anderson, J. R., Garner, C., de Groh, K. et al., "An Overview of the Results from the 30,000 Hr Life Test of Deep Space 1 Flight Spare Ion Engine," Presented at the 40th AIAA/ASME/SAE/ASEE Joint Propulsion Conference, AIAA Paper 2004-3608, Ft. Lauderdale, FL, July 11-14, 2004.

[12] Welander, B., Carpenter, C., de Grys, K. H., Hofer, R. R., Randolph, T. M. et al., "Life and Operating Range Extension of the BPT-4000 Qualification Model Hall Thruster," Presented at the 42nd AIAA/ASME/SAE/ASEE Joint Propulsion Conference, AIAA Paper 2006-5263, Sacramento, CA, July 9-12, 2006.

[13] Fife, J. M., "Hybrid-PIC Modeling and Electrostatic Probe Survey of Hall Thrusters," Ph.D. Thesis, Aeronautics and Astronautics, Massachusetts Institute of Technology, 1998.

[14] Parra, F. I., Ahedo, E., Fife, J. M., and Martinez-Sanchez, M., "A Two-Dimensional Hybrid Model of the Hall Thruster Discharge," Journal of Applied Physics (accepted for publication).

[15] Mikellides, I. G., Katz, I., Goebel, D. M., and Polk, J. E., "Hollow Cathode Theory and Experiment. II. A Two-Dimensional Theoretical Model of the Emitter Region," Journal of Applied Physics **98** (113303) (2005).

[16] Mikellides, I. G., Katz, I., Goebel, D. M., and Polk, J. E., "Theoretical Model of a Hollow Cathode Plasma for the Assessment of Insert and Keeper Lifetimes," Presented at the 41st AIAA/ASME/SAE/ASEE Joint Propulsion Conference, AIAA Paper 2005-4234, Tucson, AZ, July 10-13, 2005.

[17] Gamero-Castano, M. and Katz, I., "Estimation of Hall Thruster Erosion Using HPHALL," Presented at the 29th International Electric Propulsion Conference, IEPC Paper 2005-303, Princeton, NJ, Oct. 31-Nov. 4, 2005.

[18] Yamamura, Y. and Tawara, H., "Energy Dependence of Ion-Induced Sputtering Yields from Monatomic Solids at Normal Incidence," Atomic Data and Nuclear Data Tables **62**, 149-253 (1996).

[19] Garnier, Y., Viel, V., Roussel, J. F., and Bernard, J., "Low-Energy Xenon Ion Sputtering of Ceramics Investigated for Stationary Plasma Thrusters," Journal of Vacuum Science and Technology A **17** (6), 3246-3254 (1999).

[20] Hagelaar, G. J. M., Bareilles, J., Garrigues, L., and Bouef, J. P., "Role of Anomalous Electron Transport in a Stationary Plasma Thruster Simulation," Journal of Applied Physics **93** (1), 67-75 (2003).

[21] Koo, J. W. and Boyd, I. D., "Modeling of Anomalous Electron Mobility in Hall Thrusters," Physics of Plasmas **13** (033501) (2006).

[22] Arkhipov, B. A., Krochak, L. Z., Kudriavtsev, S. S., Murashko, V. M., and Randolph, T., "Investigation of the Stationary Plasma Thruster (SPT-100) Characteristics and Thermal Maps at the Raised Discharge Power," Presented at the 34th AIAA/ASME/SAE/ASEE Joint Propulsion Conference, AIAA Paper 98-3791, Cleveland, OH, July 13-15, 1998.

[23] Arkhipov, B. A., Krochak, L. Z., and Maslenikov, N. A., "Thermal Design of the Electric Propulsion System Components: Numerical Analysis and Testing at Fakel," Presented at the 34th AIAA/ASME/SAE/ASEE Joint Propulsion Conference, AIAA Paper 98-3489, Cleveland, OH, July 13-15, 1998.

[24] Sazhin, O. V., Borisov, S. F., and Sharipov, F., "Accommodation Coefficient of Tangential Momentum on Atomically Clean and Contaminated Surfaces," Journal of Vacuum Science and Technology A **19** (5), 2499-2503 (2001).

[25] Bird, G. A., *Molecular Gas Dynamics and the Direct Simulation of Gas Flows*, 1st ed. (Clarendon Press, Oxford, 1994).

[26] Gombosi, T. I., *Gaskinetic Theory*. (Cambridge University Press, Cambridge, 1994).

[27] Hofer, R. R., "Development and Characterization of High-Efficiency, High-Specific Impulse Xenon Hall Thrusters," Ph.D. Dissertation, Aerospace Engineering, University of Michigan, 2004. (Also NASA/CR-2004-213099)

[28] Hargus, W. A. and Cappelli, M. A., "Interior and Exterior Laser-Induced Fluorescence and Plasma Measurements within a Hall Thruster," Journal of Propulsion and Power **18** (1), 159-168 (2002).

[29] Bonnet, J., "LIF-Doppler Velocity Measurement of Xenon Atoms in a Spt50," Presented at the 28th International Electric Propulsion Conference, IEPC Paper 2003-300, Toulouse, France, Mar. 17-23, 2003.

[30] Boeuf, J. P. and Garrigues, L., "Low Frequency Oscillations in a Stationary Plasma Thruster," Journal of Applied Physics **84** (7) (1998).

[31] Boeuf, J. P., Garrigues, L., and Pitchford, L. C., in *Electron Kinetics and Applications of Glow Discharges*, edited by Kortshagen, U. and Tsendin, L. (Plenum Press, 1998).

[32] Ahedo, E., Gallardo, J. M., and Martinez-Sanchez, M., "Effects of the Radial Plasma-Wall Interaction on the Hall Thruster Discharge," Physics of Plasmas **10** (8), 3397-3409 (2003).

[33] Choueiri, E. Y., "Plasma Oscillations in Hall Thrusters," Physics of Plasmas **8** (4), 1411-1426 (2001).

[34] Haas, J. M., "Low-Perturbation Interrogation of the Internal and near-Field Plasma Structure of a Hall Thruster Using a High-Speed Probe Positioning System," Ph.D. Dissertation, Aerospace Engineering, University of Michigan, 2001.

[35] Haas, J. M. and Gallimore, A. D., "Internal Plasma Potential Profiles in a Laboratory-Model Hall Thruster," Physics of Plasmas **8** (2) (2001).

[36] Haas, J. M. and Gallimore, A. D., "Considerations on the Role of the Hall Current in a Laboratory-Model Thruster," IEEE Transactions on Plasma Science **30** (2) (2002).

[37] Morosov, A. I., Esipchuk, Y. V., Tilinin, G. N., Trofimov, A. V., Sharov, Y. A. et al., "Plasma Accelerator with Closed Electron Drift and Extended Acceleration Zone," Soviet Physics Technical Physics **17** (1) (1972).

[38] Ivanov, A. A., Ivanov, A. A., and Bacal, M., "Effect of Plasma-Wall Recombination on the Conductivity in Hall Thrusters," Plasma Physics and Controlled Fusion **44**, 1463-1470 (2002).

[39] Gascon, N., Dudeck, M., and Barral, S., "Wall Material Effects in Stationary Plasma Thrusters I: Parametric Studies of an SPT-100," Physics of Plasmas **10** (10), 4123-4136 (2003).

[40] Barral, S., Makowski, K., Peradzynski, Z., Gascon, N., and Dudeck, M., "Wall Material Effects in Stationary Plasma Thrusters II: Near-Wall and in-Wall Conductivity," Physics of Plasmas **10** (10), 4137-4152 (2003).

[41] Bishaev, A. M. and Kim, V., "Local Plasma Properties in a Hall-Current Accelerator with an Extended Acceleration Zone," Soviet Physics Technical Physics **23** (9) (1978).

[42] Hagelaar, G. J. M., Bareilles, J., Garrigues, L., and Boeuf, J. P., "Two-Dimensional Model of a Stationary Plasma Thruster," Journal of Applied Physics **91** (9) (2002).

[43] Ahedo, E., Martinez-Cerezo, P., and Martinez-Sanchez, M., "One-Dimensional Model of the Plasma Flow in a Hall Thruster," Physics of Plasmas **8** (6) (2001).

[44] Janes, G. S. and Lowder, R. S., "Anomalous Electron Diffusion and Ion Acceleration in a Low-Density Plasma," Physics of Fluids **9** (6) (1966).

[45] Meezan, N. B., Hargus, W. A., and Cappelli, M. A., "Anomalous Electron Mobility in a Coaxial Hall Discharge Plasma," Physical Review E **63** (026410), 1-7 (2001).

[46] Meezan, N. B. and Cappelli, M. A., "Kinetic Study of Wall Collisions in a Coaxial Hall Discharge," Physical Review E **66** (036401), 1-10 (2002).

[47] Kim, V., "Main Physical Features and Processes Determining the Performance of Stationary Plasma Thrusters," Journal of Propulsion and Power **14** (5), 736-743 (1998).

[48] Morozov, A. I., Esipchuk, Y. V., Kapulkin, A. M., Nevrovskii, V. A., and Smirnov, V. A., "Effect of the Magnetic Field on a Closed-Electron-Drift Accelerator," Soviet Physics Technical Physics **17** (3) (1972).